CHAPTER VI
COMPLEX CARBON NANOTUBE-INORGANIC HYBRID MATERIALS AS NEXT-GENERATION PHOTOCATALYSTS

6.1 Abstract

Hybridizing carbon nanotubes (CNTs) with complex inorganic nanostructures provides a new route to designing next-generation photocatalysts. This new class of materials utilizes charge transfer processes through the CNT-inorganic interface, which reduce the electron-hole recombination rate in the photocatalyst and so greatly enhance its activity. Herein, we demonstrate this intriguing concept with the synthesis of the first complex CNT-inorganic hybrid, using titanium-silicate (TS-1) – an important industrial zeolite - as a case study. The hybrids were synthesized via a microwave-assisted solvothermal route with the aid of benzyl alcohol as a linking agent, whose non-destructive, non-covalent modification of CNTs preserves their unique electronic properties while providing maximum interfacial area. The photocatalytic performance was tested for the degradation of 4-nitrophenol (4-NP) and rhodamine B (Rh-B) under UV light as well as visible light. The hybrids showed up to 5 times higher photocatalytic activities compared with the corresponding nano-composite and the individual components as well as increased selectivity towards total degradation via ring cleavage.

(**Keywords**: TS-1 zeolite; hybrid material, photocatalytic activity)

6.2 Introduction

Water pollution has become a global concern, threatening the survival of human beings. Effluents discharged from textile industries often contain harmful dyes, such as Rh-B [1,2] as well as toxic aromatic compounds, such as 4-NP [3] — one of the most common pollutants present in industry's waste water. In recent years, the use of photocatalysis in the decomposition of pollutants has gained tremendous interest as the most promising route for purifying air and water [4,5]. The most

common heterogeneous photocatalytic systems are based on semiconductors, such as TiO_2, due to their high chemical stability and photolysis capability [6,7]. Typically, the photoactivation in semiconductors under UV irradiation involves the excitation of an electron (e^-) from the valence band to the conduction band, generating a hole (h^+) at the valence band edge. The electrons then react with oxygen to form superoxide radical ions ($O_2^{\bullet -}$), while OH^- and H_2O are available as electron donors to yield hydroxyl radicals ($HO^\bullet$); both of which are strongly oxidizing and capable of completely mineralizing organic pollutants [8].

The photocatalytic activity of the semiconductor depends on its electronic structure (i.e. band gap energy) and on its microstructure (i.e. surface area, particle size, phase composition and crystallinity). These factors are responsible for the two major limitations in photocatalysis:

1) Although a large band gap facilitates a stronger redox ability of the photo-induced electron-hole pairs, it also restricts the light absorption range of the semiconductor to the UV region. The semiconductor can be sensitized with organic dyes (i.e. in dye-sensitized "Grätzel" solar cells [9]) or with narrow-band gap semiconductors (i.e. metal chalcogenides) to extend the absorption range into the visible spectrum of light. However, these modifications are not applicable for use in the photocatalytic waster water purification, as the sensitizers typically degrade under oxidizing conditions.

2) The photocatalytic performance is limited by the lifetime of the charge carriers, which must be sufficient for them to diffuse to the semiconductor's surface where they react with oxygen and water to form the photoactive species. It is thus crucial to maximize the separation of electrons and holes. However, long travel distances in large crystal sizes and the presence of defects significantly increase the probability of volume or surface recombination processes and consequently reduce the photocatalytic activity.

One of the most promising approaches to overcome these limitations is the hybridization of the semiconductor photocatalyst with other inorganic or organic compounds. As an example, the photocatalytic efficiency of TiO_2 was improved by combining it with activated carbon into nanocomposites [10-13]. Even more

promising, but as yet mostly unknown, are carbon nanotubes (CNTs) – inorganic hybrid materials, a new class of multifunctional materials [14]. In contrast to nano-composites (CNTs are mechanically dispersed in an inorganic matrix), CNT-inorganic hybrids (CNT are coated by a thin inorganic layer) combine their properties in a way that creates new properties distinct from those of either building block. A synergistic effect is expected through size domain effects and charge transfer processes through the CNT- inorganic interface. Although still in a very early stage of research, CNT–inorganic hybrids have shown increased sensitivities in gas sensors (SnO_2), improved efficiencies in photovoltaics (ZnO), and enhanced capacities in supercapacitors (MnO_2, RuO_2) [14]. In addition, recent studies have revealed that the addition of CNTs to TiO_2 noticeably enhanced its photocatalytic activity for the photolysis of water [15] and the oxidation of acetone [16], methanol [17], and phenol [18], and propene [19].

Although very encouraging, these results are preliminary and require more in-depth evaluation. Hence, the main objectives for this work are: (i) to assess the importance of the CNT-inorganic interface by maximizing the hybrids' interfacial area and thoroughly comparing their photocatalytic performance with that of nano-composites; and (ii) to examine changes in morphology (i.e. particle size, crystallinity) as a possible source for the improved photocatalytic properties in CNT hybrids. Herein, we employ a simple and versatile in-situ process using benzyl alcohol as a linking agent [20], which in contrast to above mentioned works has enabled continuous, uniform coatings with maximum interfacial area. Titanium silicate (TS-1) is chosen as a case study, due to its outstanding performance as a heterogeneous catalyst in epoxidation and oxidative dehydrogenation reactions [21], but also as a exceptional photocatalyst for the decomposition of dibenzothiophene [22] and 4-NP [23], and the reduction of CO_2 to CH_4 and CH_3OH [24]. We investigate the performance of CNT-TS-1 hybrids and nano-composites with various CNT concentrations for the decomposition of 4-NP and Rh-B under UV and visible light. The successful deposition of TS-1 on CNTs also marks the first synthesis of complex CNT-inorganic hybrids and demonstrates the versatility of the benzyl alcohol route.

6.3 Experimental

6.3.1 Carbon Nanotubes

Multi-walled carbon nanotubes (CNTs) were grown via a modified CVD process in a tube furnace reactor using ferrocene as the catalyst precursor and toluene as the feedstock. 4 wt% ferrocene was dissolved in 25 ml toluene and injected into an argon gas stream through a pre-heated injector (180°C) at a rate of 5.4 mL per h. The reaction was carried out in a quartz tube at 760°C. The average outer diameter of the nanotubes was 70 nm, the length was between 20 and 30 mm. Prior to their use in the hybrids, the as-grown CNTs were heated in argon at 2000°C for about 5 h.

6.3.2 TS-1 Reference

Silatrane and titanium glycolate are low cost and moisture-stable precursors and their synthesis is described in detail elsewhere [25,26]. In brief, for silatrane, a mixture of 6 g of SiO_2 (Sigma Aldrich) and 18.6 g of triethanolamine (TEA) was stirred vigorously in 100 mL ethylene glycol and heated to 200°C for 10 h. For titanium glycolate, 2 g of TiO_2 (Sigma Aldrich) was mixed with 3.65 g of triethylenetetramine (TETA), added to 25 mL ethylene glycol and heated to 200°C while stirring for 24 h. The resulting solution was centrifuged to separate the unreacted TiO_2. In both cases, excess solvent was removed in vacuum and the resulting white precipitates washed with acetonitrile and dried at room temperature. The two precursors were then mixed with NaOH, H_2O and tetrapropylammonium bromide (TPA^+), so that the final molar ratio for the reaction mixture was Ti:Si: TPA^+:NaOH = 1:20:2:8. The solution was stirred at room temperature for 60 h and subsequently heated in microwave at 150°C for 1.5 h. The product was filtered, washed with distilled water, dried at 60°C overnight and finally calcined at 550°C in argon atmosphere for 6 h.

6.3.3 TS-1/CNT Nano-Composite

It was produced by mechanically mixing the TS-1 reference and the purified CNTs (30 wt%) with the aid of a grinding mortar.

6.3.4 CNT-TS-1 Hybrids

The purified CNTs were coated with TS-1 via an in-situ sol-gel process, using ethanol as the solvent and water as the gelator. Benzyl alcohol (BA) was added as a linking agent to ensure better interaction with the hydrophobic CNTs [20]. In a typical experiment, the CNTs were dispersed in ethanol with the aid of ultrasonication for 10 min. BA and water were then added and the solution was kept stirring at room temperature. Silatrane, titanium glycolate, sodium hydroxide, water, and TPA^+ were mixed using the same concentrations as for the TS-1 reference and immediately added to the CNT suspension. The concentration of CNTs was varied from 5 to 50 wt% with respect to the expected mass of TS-1. The final suspension was aged at room temperature for 60 h and subsequently heated in microwave at 150°C for 1.5 h. The product was washed with distilled water, dried at 60°C overnight and calcined at 550°C in argon atmosphere for 6 h.

6.3.5 Characterization

The samples were characterized with EDS using JSM 580LV JEOL Japan, and X-ray diffraction (XRD) using a Bruker D8 Advance with Cu-K_α radiation, 40 kV and 40 mA, λ = 1.5406 Å. The average crystal size d of TS-1 zeolite was determined by Scherrer's equation for a given phase θ and FWHM (full width at half maximum, β), after correcting the instrumental broadening:

$$d = 0.89\lambda/(\beta\cos(\theta)) \quad (1)$$

The morphology was studied by high resolution scanning electron microscopy (SEM), using a JEOL 6340F FEG-SEM. UV-Vis spectroscopy was performed on pelletized samples in the reflectance mode, using a Perkin Elmer LAMBDA 850 spectrophotometer with an integrating sphere.

6.3.6 Photocatalytic Testing

The samples were tested for the photocatalytic decomposition of 4-NP and Rh-B under both UV (λ = 254 nm, 6 W) and visible (72 W, cutoff ~ 420 nm) lights. Typically, 60 mG of the samples were added into a quartz beaker containing 100 mL of distilled water with either 4 mG L^{-1} Rh-B solution (Solution 1), or 20 mG L^{-1} of 4-NP and 30 mmol L^{-1} of H_2O_2 (Solution 2). The suspensions were stirred in the dark for 30 min to ensure equilibrium of the dye adsorption on the surface of the

photocatalysts. Upon illumination, an aliquot part of the solution was removed every 20 min and centrifuged and analyzed by UV-Vis.

6.4 Results and Discussion

Multi-walled CNTs were grown by CVD (see experimental section) with an average diameter of approximately 70 nm and lengths of up to 50 mm (Figure 6.1 (a)). Residual iron catalyst, typically encapsulated within the CNTs [27,28], and any present amorphous carbon were effectively removed upon annealing in argon at 2000°C. This procedure also reduces the number of structural defects in the sidewalls of CNTs, which – in turn - increases their hydrophobicity. Consequently, the purified CNTs are less likely to attract hydrophilic inorganic compounds without the aid of chemical functionalization. The most common route to functionalize CNTs is boiling them in strong oxidizing acids, such as HNO_3 and H_2SO_4. Such a harsh chemical treatment typically introduces hydrophilic functional groups, such as hydroxyl and carboxyl groups, but does, however, not provide sufficient control over their number, type and location (i.e. sidewalls vs tip). As a consequence, the metal oxide coatings in previous works were often irregular and incomplete and hence not ideal for the present study.

The use of benzyl alcohol as a linking agent, as recently demonstrated [20], provides a simple and versatile route to coat purified CNTs with metal oxides without the need for chemical treatments. In this process, benzyl alcohol adsorbs on the CNT surface via π–π interactions with its benzene ring and renders it hydrophilic by providing a high density of hydroxyl groups [29]. The metal-organic precursor then reacts with the hydroxyl groups of benzyl alcohol and so deposits directly onto the CNT surface. In this work, we applied this process for the deposition of the more complex TS-1 onto CNTs. The need for two precursors, however, adds an additional complexity to this process, which requires both, a uniform coating as well as the correct composition of TS1 without phase separation. The key is the simultaneous addition of both precursors to the BA-modified CNT suspension.

Figure 6.1 (b) and (c) show typical SEM images for the CNT-TS-1 hybrid, synthesized with 30 wt% CNTs, and reveal that the CNTs were indeed covered

completely by a layer of small particles) uniform in size (18–20 nm) and regular in shape. For comparison, we synthesized a TS-1 reference sample without CNTs but under the same process conditions. This sample consisted of large aggregates of TS-1 particles with diameters between 80–100 nm (Figure 6.1 (d)). The size of the particles in the reference is thus considerably larger than that in the hybrid, which suggests a growth-suppressing role of CNTs. This is in line with previous results, which showed that CNTs can hinder the growth of TiO_2 particles as far as 50 nm away from their surface [30]. Furthermore, the thickness of the coating can be controlled by adjusting the CNT weight percentage with respect to the amount of inorganic precursor in the reaction mixture. In the present case, the average outer diameter of the CNT-TS1 hybrid with 30 wt% CNTs is approximately 160 nm, which — deducing the average diameter of CNTs of 70 nm — amasses to an average thickness of the coating of about 45 nm. Upon varying the CNT concentration from 5 to 50 wt%, the outer diameters changed from approximately 200 to 120 nm, respectively. In addition to the CNT-TS-1 hybrids, we mechanically mixed the TS-1 reference with 30 wt% CNTs with the intention to create a nano-composite with minimum interfacial area. Figure 1e confirms that the CNTs were merely surrounded by large agglomerates of TS-1 particles with a diameter of 80–100 nm, seemingly without significant physical contact between the two components.

Figures 6.2 (A-(a)) and 6.2 (A-(f)) show the X-ray diffraction pattern for the two reference samples and confirm the presence of TS-1 (ICSD no. 92536) as well as CNTs (with its 002 and 100 reflections). The average crystal size of TS-1 was calculated with Scherrer's equation to be 85 nm, which fits well with the observed particle sizes in SEM (Figure 6.1 (b)). The pattern in Figure 6.2 (A-(e)) belongs to the nano-composite (30% wt CNTs) and shows the superposition of both components' diffractions and a similar crystal size as for the TS-1 reference. The situation is markedly different for the hybrids, whose XRD patterns are shown in Figures 6.2 (A-(b),(c),(d)) for three CNT concentrations (5, 30 and 50 wt%). All hybrids exhibit the characteristic CNT diffractions. However, in contrast to the sharp peaks seen in the TS-1 reference and the nano-composite, the hybrids show very broad peaks at positions similar to those of TS-1. EDS analysis confirmed the presence of Si and Ti on the surface of CNTs and provides a Ti:Si ratio of 0.049,

which matches the expected ratio for TS-1. A closer look with XRD reveals that the peaks broaden with increasing CNT concentration, corresponding to crystal sizes of 23, 14, and 6 nm for the hybrids containing 5, 30, and 50 wt% CNTs, respectively, which is in good agreement with the particle sizes observed by SEM. Therefore, the combined results from SEM, EDS and XRD confirm that the coatings are indeed composed of TS-1. Furthermore, the use of benzyl alcohol has enabled the synthesis of CNT-hybrids with maximum interfacial area and excellent control of morphology.

Figure 6.2 (B) shows the UV–Vis absorption spectra for the various samples. As expected, CNTs absorb in the entire visible spectrum. In contrast, the TS-1 reference sample strongly absorbs in the UV range with a sharp absorption band edge just below 300 nm. The spectra for the hybrids and the nano-composite (30 wt%, Fig 6.2 (A-(e)) combine the absorption characteristics of both individual components. However, the hybrids show an additional, weak absorption peak at around 300 nm, which increases with increasing CNT concentration. This feature may be associated with charger transfer processes, whose identification and quantification, however, require further studies. Another characteristic of the CNT hybrids is the slight blue-shift of the absorption band edge with respect to the TS-1 reference sample. This feature appears to be stronger with increasing CNT concentration, i.e. with decreasing TS-1 crystal size, and is likely to be associated with quantum-size effects in small TS-1 nanoparticles [31].

The photocatalytic performance of the samples was evaluated for the degradation of 4-NP (in the presence of H_2O_2) and Rh-B, using UV light (λ = 254 nm) as well as visible light (cut-off = 420 nm). The photocatalytic activity is generally taken as the rate of decrease of the absorbance (*aka* dye concentration) over irradiation time. The changes in maximum absorbance (400 nm for 4-NP, 560 nm for Rh-B) with reaction time are shown in Figure 6.3. For all samples, the concentrations of 4-NP and Rh-B decreased exponentially, indicating a first-order reaction. The values for conversion (after 40 min) and initial rate (from the slope in the log(C) vs time t plot) based on the number of Ti sites are shown in Figures 6.4 (a) and (b) and summarized in table 6.1. The results clearly demonstrate that the uncoated CNTs were almost inactive under all reaction conditions, while the TS-1 reference caused a small decrease in dye concentration. The nano-composite (30

wt%) was slightly more active than the reference sample. In contrast, all hybrid samples showed considerably larger conversions and greatly enhanced activities over their individual components. Interestingly, the highest activities were observed for the hybrid with 30 wt% CNTs, which was nearly 6 times as active as the TS-1 reference.

There are two possible origins for the improved photocatalytic activity in the hybrids: The first explanation is purely physical and is based on the fact that the particle sizes of TS-1 in the hybrids (6, 14, 23 nm for 50, 30, and 5 wt% CNTs, respectively) are significantly smaller than in the nano-composite (85 nm). A smaller crystal size indicates a larger surface area, which allows the conversion of more reactants on the surface of the catalyst. In first approximation, the decrease in particle size with increasing CNT concentration in the hybrids correlates with the observed increase in photocatalytic activity up to 30 wt% CNTs. At higher CNT concentrations, however, the activities dropped, although the particle sizes decreased further. This indicates that the contribution of the particle size was likely not the only important factor.

The second explanation involves charge transfer processes through the CNT-TS-1 interface, which may proceed in two ways: (1) The CNTs may act as photosensitizers: In this model, photo-induced electrons are transferred from CNTs to the CNT-TS-1 interface and injected into the TS-1 conduction band. Simultaneously, a hole forms by an electron migrating from the TS-1 valence band to the CNT. This charge transfer triggers the formation of the reactive radical species required for the degradation of the organic compound. A similar electron transfer has been observed between various carbon materials and TiO_2. [32]. (2) CNTs may act as electron acceptors: Electrons are photoexcited in TS-1 (or the adsorbed dye) and transferred to CNTs, leaving holes behind in the valence band. Consequently, this charge separation retards the electron-hole recombination and so improves the photocatalytic activity. A similar charge transfer mechanism has been suggested for semiconducting quantum dots, such as CdS and CdSe [33-36].

To clarify whether the particle size or charge transfer processes through the interface are responsible for the observed synergistic effect, we processed the CNT-TS1 hybrid with 30 wt% CNTs by high-speed ball milling for 6 hours. Our intention

was to separate the TS-1 coating from the CNTs and to create a new sample with the same particle size of TS-1 as in the CNT-TS-1 hybrid but without physical contact between the two components. The SEM image in Figure 1f shows that most of the coating was broken away from the CNTs, while XRD analysis confirmed that the average crystal size (13 nm) remained virtually unchanged. The photocatalytic activities of this ball-milled sample for both, 4-NP and Rh-B, were greatly reduced to almost the same values as for the nano-composite (Figure 6.4 (b), Table 6.1). This clearly demonstrates that a close proximity of the two components and the associated charge transfer processes are crucial for the enhanced photocatalytic performance in CNT-TS-1 hybrids. Further studies are required to assess the extent of the charge transfer processes.

Figures 6.5 (c) and (d) shows the changes in UV-VIS absorbance with progressing irradiation time for 4-NP (in UV) and Rh-B (in visible light), using the CNT-TS-1 hybrid with 30 wt% CNTs as the photocatalyst. The decrease of 4-NP is considerably stronger under UV irradiation than in visible light (Figure 6.3). This is characteristic for the classical *photocatalytic pathway*, in which the photoexcited electrons and holes in the semiconductor react with water and molecular oxygen to form the reactive superoxide and hydroxide radical species (Figure 6.5 (a)). Presumably, these species attack the 4-NP in the solution via a fast direct cleavage of the aromatic rings. In this scenario, however, the photocatalytic activity is limited to UV illumination by the relatively large band-gap energy of the semiconductor.

The situation is different for Rh-B, where the rate of decrease is slightly larger upon irradiation in visible light compared to UV illumination. In this case, the degradation of Rh-B most likely proceeds via the photosensitization pathway, in which the dye sensitizes its own oxidative transformation by the direct formation of the oxidizing OH radicals [37]. In other words, the excited dye injects electrons into the conduction band of the semiconductor, where they are transferred to surface-adsorbed O_2 molecules to yield the superoxide (Figure 6.5 (b)). Due to the proximity of the reactive species and the dye adsorption sites, the photooxidation of the dye is a surface occurring process and so depends on its adsorption mode. Chen et al showed that Rh-B adsorbs on TiO_2/SiO_2 via positively charged diethylamino groups [38]. Due to their proximity to the catalyst's surface, the active oxygen species

preferentially attack these diethylamino groups rather than the aromatic rings. Hence, the photosensitization pathway, although enabling visible light photocatalysis, results in a slower and stepwise degradation of Rh-B via deethylation.

It is relatively easy to distinguish between the two degradation mechanisms by following the color change for the dye solution as the reaction proceeds. A color change from purple to yellow, associated with a small blue-shift of the UV-Vis absorption peak, typically indicates deethylation, while a fading color without peak shift corresponds to the direct decomposition via ring cleavage. As expected, we observed a slight color change from purple to orange in the case of the TS-1 reference, while the purple color gradually disappeared in presence the CNT-TS-1 hybrid (Figure 6.5 (d)). This indicates that the visible light photodegradation of Rh-B with hybrids proceeds via fast direct degradation via ring cleavage in contrast to pure TS-1, which favored the deethylation. The reason for this preference in the photodegradation mechanism is currently under detailed investigation.

6.5 Conclusions

This work demonstrates the successful synthesis of the first complex CNT-inorganic hybrid, using titanium silicate (TS-1) as a case study. The use of benzyl alcohol as a linking agent has enabled the deposition of a uniform, continuous layer of TS-1 on CNTs, so creating hybrids with maximum interfacial contact area. This simple and versatile "benzyl alcohol route" can potentially be applied to synthesizing CNT hybrids with a wide range of inorganic compounds, ranging from transition and rare earth metal oxides to oxide solid solutions and metal organic frameworks, without the need for covalent functionalization.

This work further demonstrates the exceptional photocatalytic performance of the CNT-TS-1 hybrids for the degradation of 4-NP and Rh-B under both, UV and visible light irradiation. The highest photocatalytic activity was observed for the CNT-TS-1 hybrids with 30 wt% CNTs, which was up to 6 times higher than for the corresponding nano-composite and both individual components. In addition, the hybrids selectively degraded Rh-B via cleavage of the aromatic rings, in contrast to pure TS-1, which preferred the slower degradation via deethylation. The superior

performance of the hybrids origins in charge transfer processes through the CNT-TS1 interface effectively reduces the electron-hole recombination rate in the photocatalyst, and so enhances its activity. Further studies are currently carried out to evaluate the nature and extent of this synergistic effect.

6.6 Acknowledgements

This research work was supported by the Center for Petroleum, Petrochemicals and Advanced Materials (C-PPAM), the Ratchadapisake Sompote Fund, and the Thailand Research Fund (TRF). D. E. is grateful to the Austrian Academy of Sciences for financial support via the APART Research Fellowship.

6.7 References

1. N. Venkatachalam, M. Palanichamy, V. Murugesan, "Sol–gel preparation and characterization of alkaline earth metal doped nano TiO_2: Efficient photocatalytic degradation of 4-chlorophenol", *J. Mol. Catal. A: Chem.*, **273**, 177-185 (2007).
2. Y. Li, S. Sun, M. Ma, Y. Ouyang, W. Yan, "Kinetic study and model of the photocatalytic degradation of rhodamine B (RhB) by a TiO_2-coated activated carbon catalyst: effects of initial RhB content, light intensity and TiO_2 content in the catalyst", *J. Chem. Eng.*, **142**, 147-155 (2008).
3. D. Carriazo, M. Addamo, G. Marci, C. Martin, L. Palmisano, V. Rives, "Preparation and Characterisation of TiO_2 (anatase) Supported on TiO_2 (Rutile) Catalysts Employed for 4-Nitrophenol Photodegradation in Aqueous Medium and Comparison with TiO_2 (anatase) Supported on Al_2O_3", *Appl. Catal. B: General* : Environ **20**, 29-45 (1999).
4. L. Andronic, A. Duta, "TiO_2 thin films for dyes photodegradation", *Thin Solid Films*, **515**, 6294-6297 (2007).
5. P. Evans, S. Mantke, A. Mills, A. Robinson, D. W. Sheel, "A comparative study of three techniques for determining photocatalytic activity", *J. Photochem. Photobiol. A*, **188**, 387-391 (2007).

6. D. A. Tryk, A. Fujishima, K. Honda, "Recent topics in photoelectrochemistry: achievements and future prospects", *Electrochim. Acta*, **45**, 2363-2376 (2000).
7. A. T. Fujishima, T. N. Rao, D. A. Tryk, "Titanium dioxide photocatalysis", *J. Photochem. Photobiol. C, Photochem. Rev.*, **1**, 1-21 (2000).
8. O. M. Alfano, M. I. Cabrera, A. E. Cassano, "Photocatalytic Reactions Involving Hydroxyl Radical Attack", *J. Catal.*, **172**, 370-379 (1997).
9. B. O'Regan, M. Graetzel, "A low-cost, high-efficiency solar cell based on dye-sensitized colloidal TiO_2 films", *Nature*, **353**, 737-740 (1991).
10. J. Matos, J. Laine, J.-M. Herrmann, "Synergy effect in the photocatalytic degradation of phenol on a suspended mixture of titania and activated carbon", *Appl. Catal. B: Environmental*, **18**, 281-291 (1998).
11. C. G. Silva, J. L. Faria, "Photochemical and photocatalytic degradation of an azo dye in aqueous solution by UV irradiation", *J. Photochem. Photobiol. A*, **155**, 133-143 (2003).
12. G. Colón, M. C. Hidalgo, M. Macías, J. A. Navío, J. M. Doña, "Influence of residual carbon on the photocatalytic activity of TiO_2/C samples for phenol oxidation", *Appl Catal B: Environ,* **43**, 163-173 (2003).
13. B. Tryba, A. W. Morawski, M. Inagaki, "Application of TiO_2-mounted activated carbon to the removal of phenol from water", *Appl Catal B: Environ*, **41**, 427-433 (2003).
14. D. Eder, "Carbon Nanotube-Inorganic Hybrids", *Chem. Rev.*, **110 (3)**, 1348–1385 (2010).
15. G.-J. Wang, M.-W. Lee, Y.-H. Chen, "A TiO_2/CNT Coaxial Structure and Standing CNT Array Laminated Photocatalyst to Enhance the Photolysis Efficiency of TiO_2", *Photochem. Photobio.*, **84**, 1493-1499 (2008).
16. Y. Yu, J. C. Yu, J.-G. Yu, Y.-C. Kwok, Y.-K. Che, J.-C. Zhao, L. Ding, W.-K. Ge, P.-K. Wong, "Enhancement of photocatalytic activity of mesoporous TiO_2 by using carbon nanotubes", *Appl Catal A: Gen*, **289**, 186–196 (2005).
17. C. Dechakiatkrai, J. Chen, C. Lynam, S. Phanichphant, G. G. Wallace, "Photocatalytic oxidation of methanol using titanium dioxide/single-walled carbon nanotube composite", *J. Electrochem. Soc.*, **154**, A407-A411 (2007).

18. Y. Yao, G. Li, S. Ciston, R. M. Lueptow, K. A. Gray, "Photoreactive TiO_2/Carbon Nanotube Composites: Synthesis and Reactivity", *Environ. Sci. Technol.*, **42**, 4952 (2008).
19. N. Bouazza, M. Ouzzine, M. A. Lillo-Ródenas, D. Eder, A. Linares-Solano, "TiO_2 nanotubes and CNT–TiO_2 hybrid materials for the photocatalytic oxidation of propene at low concentration", *Appl Catal B: Environ*, **92**, 377-383 (2009).
20. D. Eder, A. H. Windle, "Carbon–Inorganic Hybrid Materials: The Carbon-Nanotube/TiO_2 Interface", *Adv. Mater.*, **20**, 1787-1793 (2008).
21. G. N. Vayssilov, "Structural and physicochemical features of titanium silicalites", *Catal. Rev.*, **39**, 209-251 (1997).
22. Z. Juan, Z. Dishun, Y. Liyan, L. Yongbo, "Photocatalytic oxidation dibenzothiophene using TS-1", *Chem. Eng. J.*, **156**, 528-531 (2010).
23. N. Phonthammachai, M. Krissanasaeranee, E. Gulari, A. M. Jamieson, S. Wongkasemjit, "Crystallization and catalytic activity of high titanium loaded TS-1 zeolite", *Mater. Chem. Phys.*, **97**, 458-467 (2006).
24. S. Yamagata, M. Nishijo, N. Murao, S. Ohta, I. Mizoguchi, "CO_2 reduction to CH_4 with H_2 on photoirradiated TS-1", *Zeolites*, **15**, 490-493 (1995).
25. P. Piboonchaisit, S. Wongkasemjit, R. Laine, "A Novel Route to Tris(silatranyloxy-*i*-propyl)amine Directly from Silica and Triisopropanolamine, Part I", *Science-Asia, J. Sci. Soc.Thailand*, **25**, 113-119 (1999).
26. N. Phonthammachai, T. Chairassameewong, E. Gulari, A. M. Jamieson, S. Wongkasemjit, "Structural and rheological aspect of mesoporous nanocrystalline TiO_2 synthesized via sol–gel process", *J. Met. Mater. Min*, **12**, 23-28 (2002).
27. D. Eder, M.S. Motta, I.A. Kinloch and A.H. Windle, "Anatase nanotubes as support for platinum nanocrystals", *Physica E*, **37**, 245–249 (2007).
28. D. Eder, M. S. Motta, A. H. Windle, "Iron-doped Pt–TiO_2 nanotubes for photo-catalytic water splitting", *Nanotechnolog*, **20**, 055602 (2009).
29. D. J. Cooke, D. Eder, J. A. Elliott, "Role of Benzyl Alcohol in Controlling the Growth of TiO_2 on Carbon Nanotubes", *J. Phys. Chem. C*, **114**, 2462–2470 (2010).

30. D. Eder, A. H. Windle, "Morphology control of CNT-TiO_2 hybrid materials and rutile nanotubes", *J. Mater. Chem.*, **18**, 2036-2043 (2008).
31. S. Klein, B. M. Weckhuysen, J. A. Martens, W. F. Maier, P. A. Jacobs, "Homogeneity of Titania-Silica Mixed Oxides: On UV-DRS Studies as a Function of Titania Content", *J. Catal.*, **163**, 489-491 (1996).
32. H.-C. Huang, G.-L. Huang, H.-L. Chen, Y.-D. Lee, "Immobilization of TiO_2 nanoparticles on carbon nanocapsules for photovoltaic applications", *Thin Solid Films*, **203**, *511-512* (2006).
33. W. D. Wang, P. Serp, P. Kalck, J. L. Faria, "Photocatalytic degradation of phenol on MWNT and titania composite catalysts prepared by a modified sol–gel method", *Appl Catal B: Environ*, **56**, 305-312 (2005).
34. D. M. Guldi, G. M. A. Rahman, V. Sgobba, N. A. Kotov, D. Bonifazi, M. "CNT−CdTe Versatile Donor−Acceptor Nanohybrids", *J. Am. Chem. Soc.*, **128**, 2315-2323 (2006).
35. I. Robel, B. A. Bunker, P. V. Kamat, "Single-Walled Carbon Nanotube-CdS Nanocomposites as Light-Harvesting Assemblies: Photoinduced Charge-Transfer Interactions", *Adv. Mater.*, **17**, 2458-2463 (2005).
36. P. V. Kamat, "Harvesting photons with carbon nanotubes", *Nano Today*, **1**, 20-27 (2006).
37. T. Wu, G. Liu, J. Zhao, H. Hidaka, N. Serpone, "Photoassisted Degradation of Dye Pollutants. V. Self-Photosensitized Oxidative Transformation of *Rhodamine B* under Visible Light Irradiation in Aqueous TiO_2 Dispersions", *J. Phys. Chem. B*, **102**, 5845-5851 (1998).
38. F. Chen, J. Zhao, H. Hidaka, Inter. "Highly selective deethylation of rhodamine B: adsorption and photooxidation pathways of the dye on the TiO_2/SiO_2 composite photocatalyst", *J. Photoenergy*, **5**, 209-217 (2003).

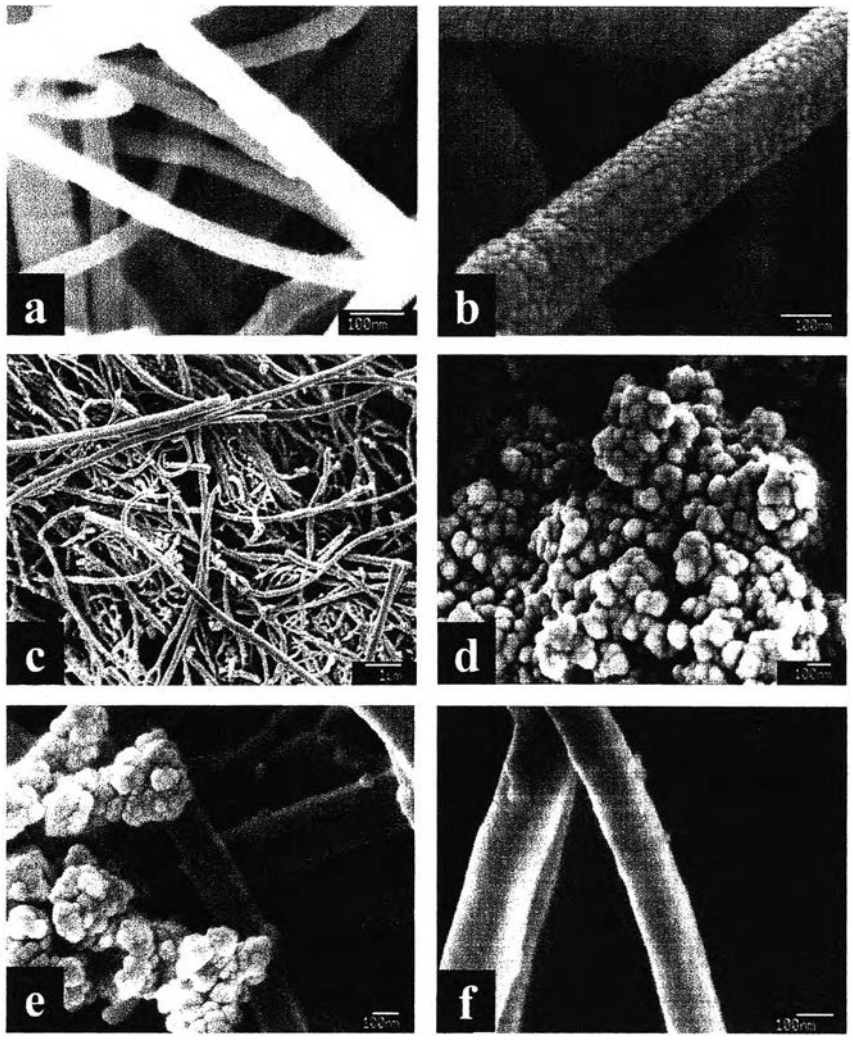

Figure 6.1 SEM images of (a) MWCNTs, (b,c) CNT-TS1 hybrids with 30 wt% CNTs, (d) the TS-1 reference sample, (e) the mechanically-mixed TS-1/CNT nano composite (30 wt% CNTs), and (f) the CNT-TS1 hybrid with 30 wt% CNTs after ball-milling.

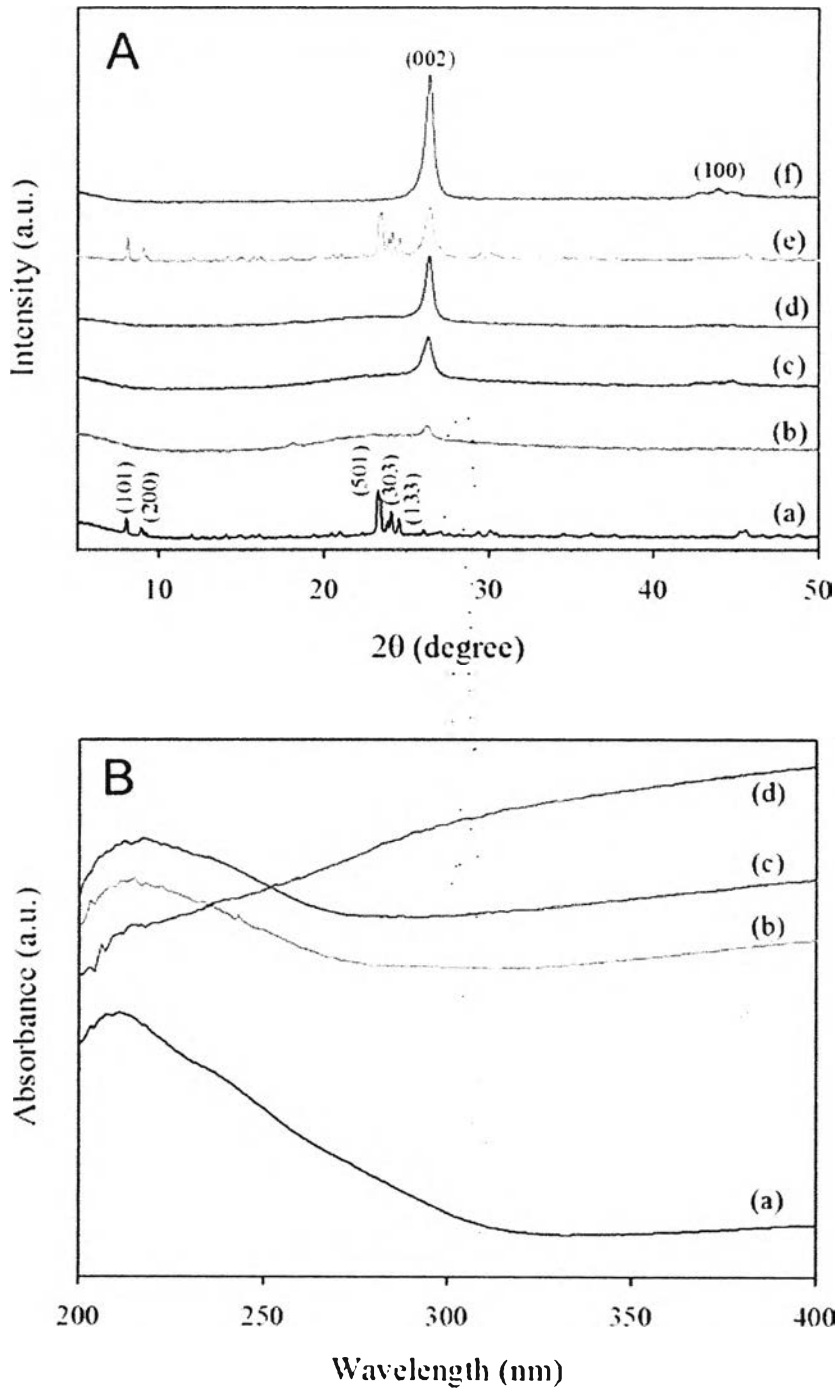

Figure 6.2 A: X-ray diffraction pattern for (a) the TS-1 reference, CNT-TS1 hybrids with a CNTs concentration of (b) 5 wt% (c) 30 wt%, and (d) 50 wt%, (e) the TS-1/CNT nano-composite, and (f) MWCNTs. B: UV-Vis spectra of (a) the TS-1 reference, (b) the CNT-TS1 hybrid with 30 wt% CNTs, (c) the TS-1/CNT nano-composite (30 wt% CNTs), and (d) MWCNTs

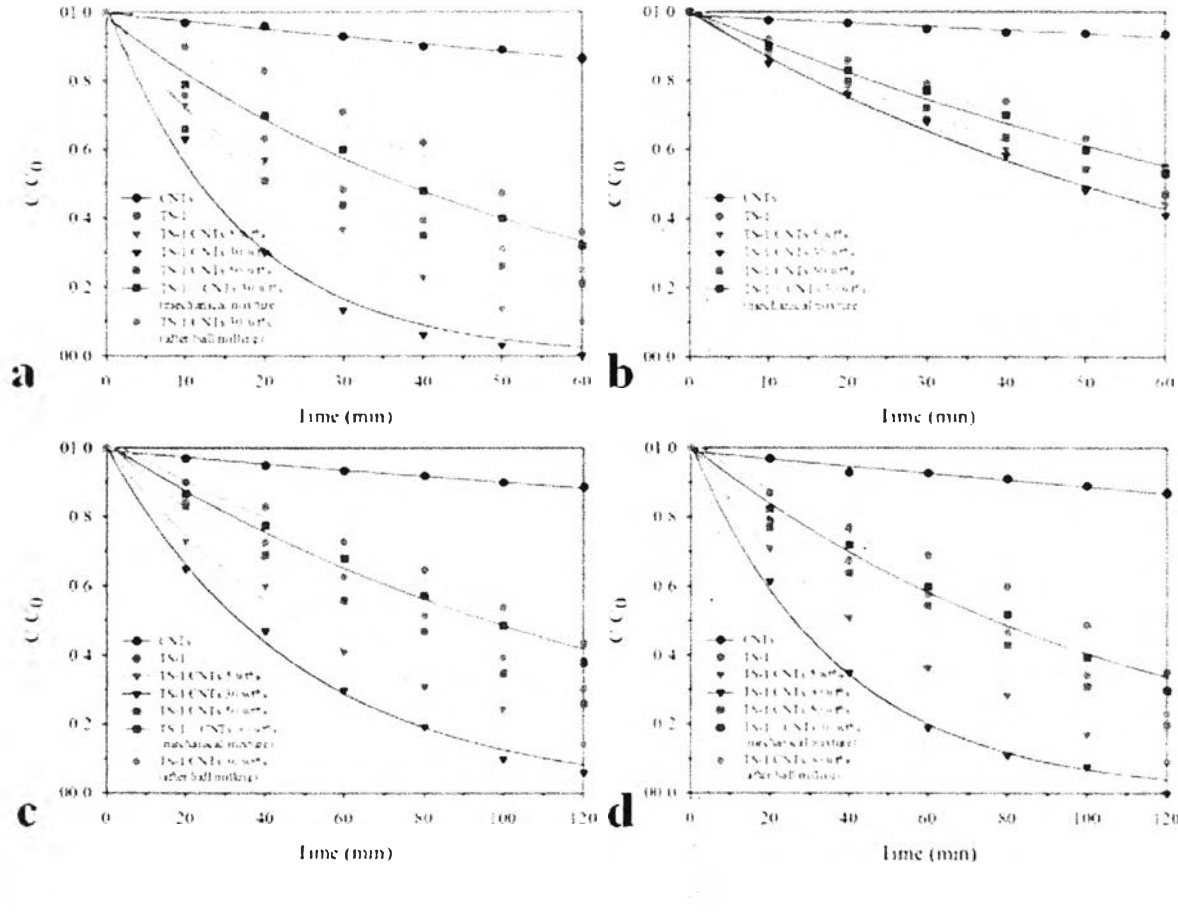

Figure 6.3 Decrease in absorbance with progressing reaction time for different catalysts for (a) 4-NP under UV light, (b) 4-NP under visible light, (c) Rh-B under UV light, (d) Rh-B under visible light.

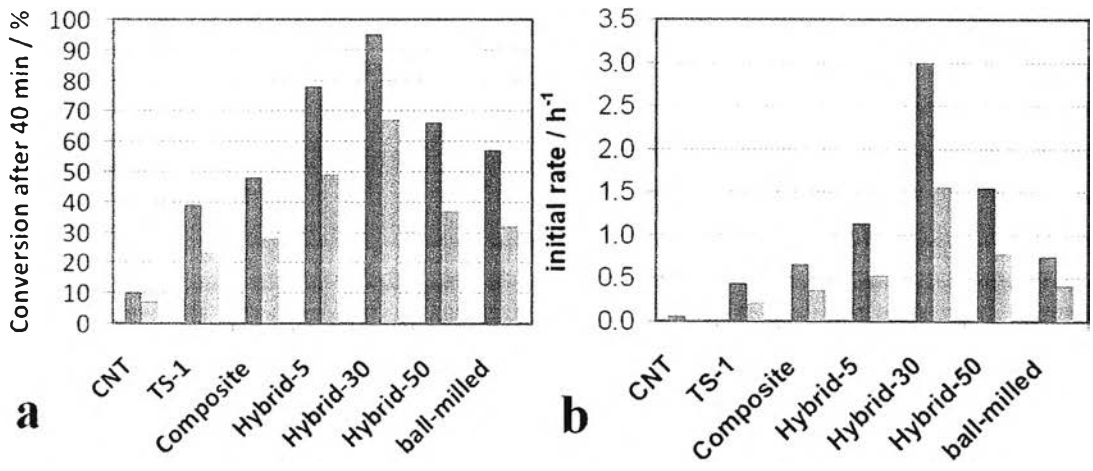

Figure 6.4 The values of different catalysts for (a) conversion after 40 min reaction time and (b) initial rate per hour. Blue: 4-NP in UV light, green: Rh-B in visible light.

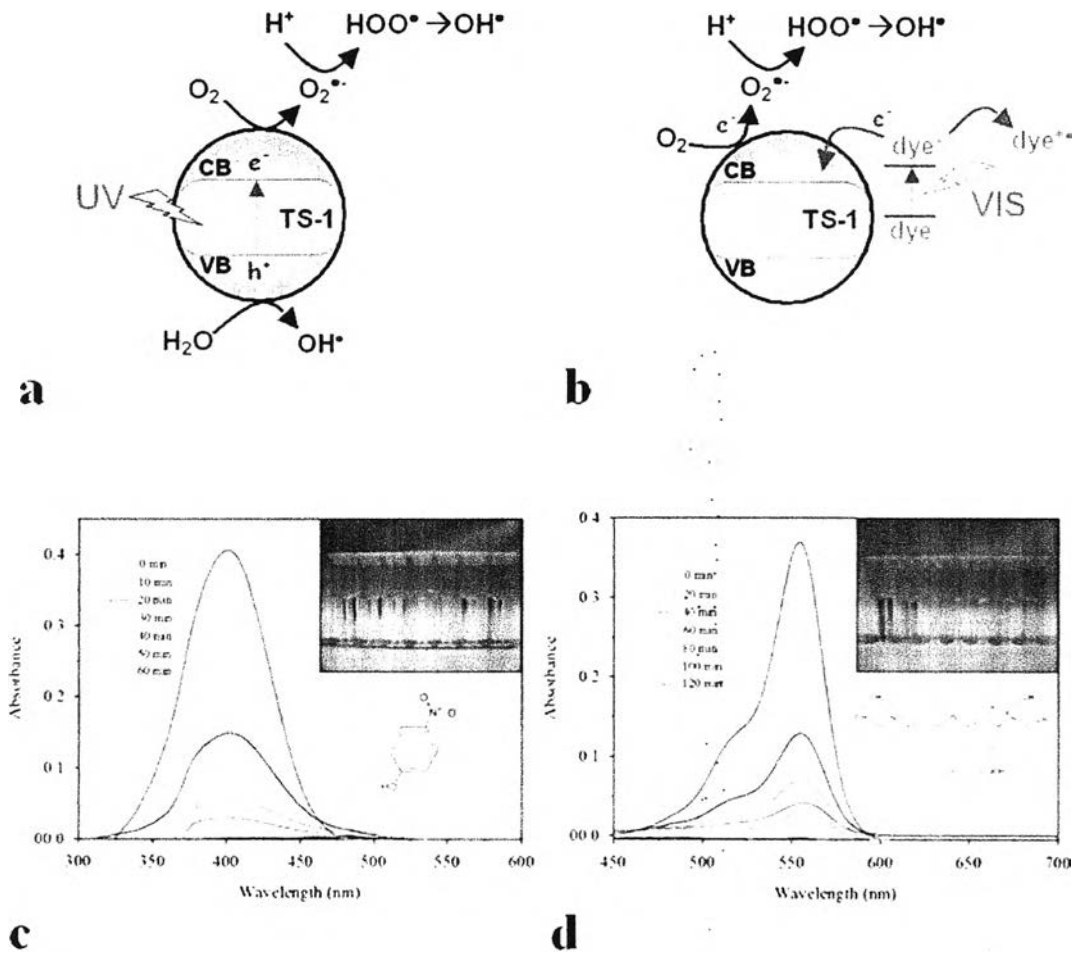

Figure 6.5 Schemes for (a) the photocatalytic mechanism under UV light and (b) the photosensitization pathway under visible light irradiation. Time-dependent UV–vis absorption spectra of (c) 4 nitrophenol under UV light, (d) rhodamine B under visible light, using the CNT-TS1 hybrid with 30 wt% CNTs. The insets show the color change with progressing reaction time.

Table 6.1 Overview of conversion values after 40 min reaction and initial rates per hour for 4-NP and Rh-B, both in UV and visible light, for all samples.

Sample	4-nitrophenol				Rhodamine B			
	UV-light		Visible light		UV-light		Visible light	
	Conversion/ % After 40 min	Initial rate h^{-1}	Conversion/ % After 40 min	Initial rate h^{-1}	Conversion/ % After 40 min	Initial rate h^{-1}	Conversion/ % After 40 min	Initial rate h^{-1}
CNT	10	0.06	5	0.03	5	0.02	7	0.02
TS-1	39	0.43	26	0.25	20	0.17	23	0.21
Nano-composite	48	0.66	3	0.36	23	0.29	28	0.36
Hybrid-5	78	1.13	40	0.38	33	0.43	49	0.53
Hybrid-30	95	3.00	43	0.63	55	0.87	67	1.56
Hybrid-50	66	1.54	36	0.65	43	0.58	37	0.78
Ball-milled	57	0.75	-	-	28	0.36	32	0.42